Quantitative Description of Ultrafiltration in a Rotating Filtration Device

Ulrich B. Holeschovsky and Charles L. Cooney
Dept. of Chemical Engineering, Biotechnology Process Engineering Center, Massachusetts Institute of Technology, Cambridge, MA 02139

A correlation was developed to quantitatively describe the flux in a high-speed rotating filtration device using a minimum set of parameters. The experimental results were found to be consistent with the concentration polarization (CP) model. Beyond a threshold pressure flux ceases to depend on membrane permeability. The CP model was modified to include the concentration dependence of the diffusivity. This approach was found to be consistent with the strong dependence of flux on pH. Protein concentration in the polarized layer adjacent to the membrane surface was estimated using a procedure that corrects for some of the inconsistencies in the methods usually applied. Four dimensionless numbers were necessary to correlate the experiments with good accuracy. Previously-reported correlations used only three dimensionless numbers. Usage of four numbers could be justified by dimensional analysis. Finally, the performance of rotary or vortex filtration was compared to that of other configurations.

Introduction

Membrane filtration is an important unit operation in downstream processing for biological products. A barrier to the application of this technology is fouling of the membrane that reduces filtration flux and recovery yield and increases maintenance requirements. Membrane fouling can be reduced in part by the use of hydrophilic membranes reducing adsorption of biomolecules on the membrane and by filtration devices minimizing concentration polarization at the membrane surface. One can generate a secondary flow called Taylor Vortices with a high-speed rotating filter in a narrow annular gap to reduce concentration polarization by increasing the removal rate of protein deposited at the membrane surface. This process is called vortex flow filtration (VFF).

The influence of membrane permeability, concentration, pH, pressure, rotating rate, fluid velocity and gap width on VFF was investigated using solutions of bovine serum albumin (BSA) ranging from 10 g/L to very high concentrations of 200 g/L. The theoretical approach modifies the commonly-used concentration polarization (CP) model and yields good agreement between experiment and theory. This treatment also allowed quantitative comparison between VFF and other configurations such as hollow-fiber or plate and frame devices. The analysis shows that filtration performance in VFF is superior to that obtainable in cross-flow filtration (CFF) devices.

Correspondence concerning this article should be addressed to C. L. Cooney.

Theory

All filtration configurations for protein ultrafiltration show a typical relation between filtration flux and transmembrane pressure. At low pressures, the flux increases proportionally to the applied pressure. This is followed by a transition, in which flux becomes less pressure-dependent. Finally, a pressure-independent zone is reached. This type of behavior is attributed to concentration polarization (the CP model). During ultrafiltration, solute is brought to the membrane surface by convection where it is rejected by the membrane. This leads to the accumulation of protein at the membrane and the formation of a concentration gradient. The protein concentration at the membrane surface can rise up to a certain limit. Further accumulation of protein causes the buildup of a concentrated protein layer, until the increased hydrodynamic resistance of this layer reduces the solvent flux; and then back-diffusion of protein balances the convective transport to the surface. Accordingly, the rate of protein removal from the surface, when

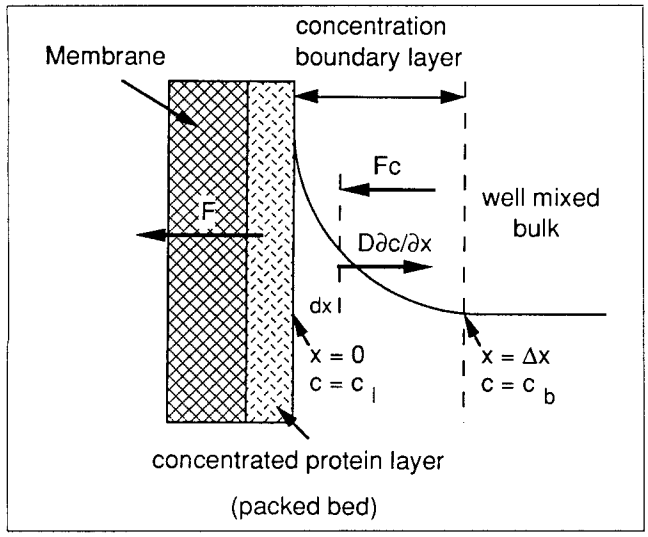

Figure 1. CP model.

Steady state is reached when the convective term is balanced by diffusion into the bulk.

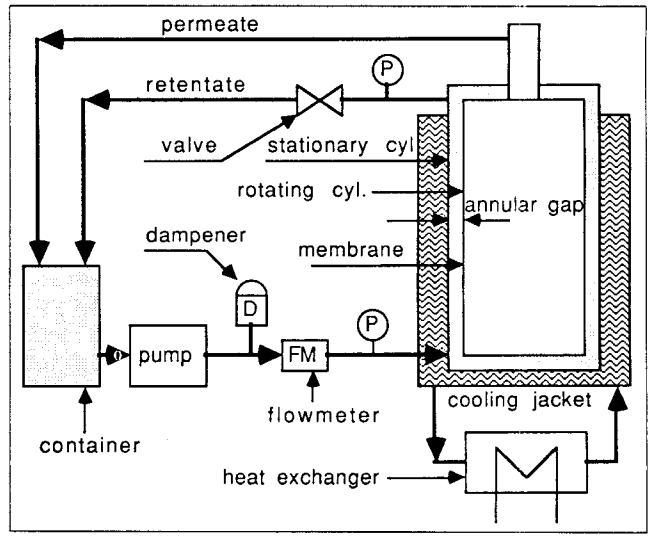

Figure 2. Experimental setup for vortex flow filtration.

p indicates pressure measurement, see text for details.

balanced by convective deposition, determines the thickness of the concentrated layer.

As depicted in Figure 1, a mass balance at steady state on a differential element yields:

$$Fc = D\frac{\delta c}{\delta x} \tag{1}$$

In the above equation, D usually is assumed constant, even though the diffusivity of proteins is a function of concentration, pH, ionic strength and solution composition. In the absence of strong long-range interactions, the concentration dependence of D can be expressed as described by Fair et al. (1978):

$$D = D^o(1 + bc) \tag{2}$$

where the factor b depends on pH, ionic strength and solution composition. Substitution of Eq. 2 in Eq. 1 leads to:

$$F = \frac{D^o}{\Delta x}\left[\ln\frac{c_l}{c_b} + b(c_l - c_b)\right] \tag{3}$$

Restating Eq. 3:

$$F = kf(c) \tag{4}$$

where $k = D^o/\Delta x$ = mass transfer coefficient evaluated with bulk solution properties, $[k]$ = m/s. Assuming D is constant ($b = 0$), $f(c)$ becomes the commonly-used expression:

$$f(c) = \ln\frac{c_l}{c_b} \tag{5}$$

To describe the mass transfer coefficient in terms of operation, design and physical properties, a dimensional analysis was conducted. The mass transfer coefficient k was assumed to be a function of kinematic viscosity ν, diffusivity D, angular speed of the inner cylinder ω, axial superficial velocity v, radius of the inner cylinder R, and hydraulic diameter $d_h = 2^*d$, where d = gap width.

Together with k there are seven parameters in the dimensions time and length. Therefore, a complete set of dimensionless numbers can contain up to five members. The parameters may be arranged and expressed conveniently as:

$$Sh = f\left(Re_t, \frac{2d}{R}, Sc, Re_a\right) \tag{6}$$

where $Sh = 2kd/D$ (Sherwood number), $Re_t = 2\omega Rd/\nu$ (tangential Reynolds number), $Sc = \nu/D$ (Schmidt number), and $Re_a = 2vd/\nu$ (axial Reynolds number).

We assume that Eq. 6 can be approximated using a constant A; thus,

$$Sh = A\ Re_t^a\left(\frac{2d}{R}\right)^b Sc^c Re_a^d \tag{7}$$

The experimental design developed here is intended to validate this relationship.

Experimental Set-Up and Equipment

A Benchmark vortex flow (VFF) filtration system (Membrex, Garfield, NJ) was used for this work. The maximum pressure rating for this system is 3.4 bar. The system was adapted to allow application of pressures up to 12.2 bar by changing the tubing and the connectors, and by using a tubular diaphragm pump. The original stationary outer cylinder was replaced by a stainless steel jacket to allow temperature control at $20 \pm 0.5°$. The temperature was measured in the gap by a thermocouple that could be screwed into the wall of the steel jacket.

Figure 2 depicts the experimental set-up. The feed is pumped into the annular gap between the two concentric cylinders. The gap width is 0.9, 2.15 and 3.3 mm. The inner cylinder (radius

2.23 cm and length 17 cm) containing the membrane rotates, while the outer one is stationary. The operating pressure in the annular gap was controlled by a regulating valve, which createsa back-pressure along the membrane to the outlet of the pump (Figure 2). The pressure was measured at the entrance and the exit of the filtration unit by means of pressure test gauges (accuracy 0.25% of full scale = 0.027 bar) as indicated in Figure 2. The axial pressure drop along the membrane was negligible, for example, < 0.2 bar. The feed rate was monitored by a flowmeter, and the permeate flux was determined by measuring the time necessary to collect a volume of several milliliters of permeate. Both permeate and retenate were recycled to maintain the bulk protein concentration constant.

As a further condition for a differential operating mode, the ratio between feed and permeate was chosen to be at least 25 so as not to change the bulk concentration in the axial direction. For a ratio of 25, the concentration of the bulk rises by 4% in the axial concentration. Assuming a linear rise as an approximation, the average concentration is 2% higher than the concentration of the feed, which was considered an acceptable error. For high protein concentrations and high feed, this minimum ratio could be maintained by using the original membrane cartridge with an area of 200 cm^2. In the case of low feed rates, especially at low protein concentrations, the cartridge filtration area was reduced from 200 cm^2 to 30 cm^2 by blocking collector channels with polypropylene on the permeate side.

The superficial axial fluid velocity v was varied from 0.46 to 14 cm/s corresponding to an axial Reynolds number from 25 to 200. The tangential velocity of the inner cylinder v_t was varied from 0.47 to 9.4 m/s corresponding to a tangential Reynolds number of 680–50,600. Aqueous solutions at pH = 7.4, 0.15 M NaCl in a 0.01 M phosphate buffer of bovine serum albumin (BSA) at 98–99% purity (Sigma, A 7906) were used for all the experiments reported here in a concentration range of 10–200 g/L. The following material properties were used in our analysis: $D = D^o(1 + bc)$ with $D^o = 5.65 \times 10^{-11}$ [m^2/s], b = 0.0019 at pH 7.4, 0.15 M NaCl, 0.01 M phosphate buffer, and $b = -0.0021$ at pH 4.7 and 0.1 M acetate buffer (Fair et al., 1978); $\mu = \mu_w \exp(2.44 \times 10^{-5} \times c^2)$, (Kozinski and Lightfoot, 1972); $\rho = 1 + 2.54 \times 10^{-4} c$, (Vilker et al., 1981).

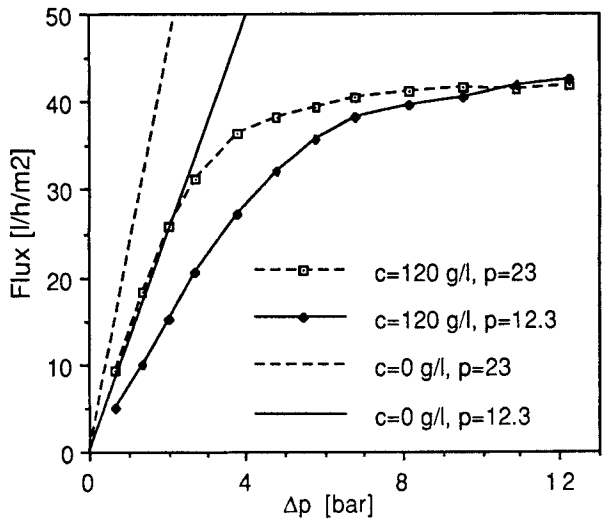

Figure 3. Flux vs. transmembrane pressure difference for different membrane permeabilities.

Rejection >99%; $Re_t = 7{,}000$; $Re_a = 50$; $d/R = 0.096$; p = permeability; [p] = L/h/m^2/bar.

The experiments were performed with Membrex MX-10 ultrafiltration membranes made of modified polyacrylonitrile. The rejection was always larger than 99% (Rejection = 1 − permeate concentration/retentate concentration). For each experiment, a freshly-prepared protein solution of 1 L was used. The typical duration of an experiment was between two and three hours, although longer experiments were performed to check for a possible decrease in flux. It was observed that steady flux was established within seconds. All data reported are the average values of 12–18 measurements with standard deviations ranging from 0.5 to 2.5%. The membrane permeability was measured after each experiment to assess the hydrodynamic resistance. The system was flushed with pure water for about five minutes and the permeability determined by measuring the water flux. In general, no decrease in permeability was detected. This can be attributed to the use of a highly-hydrophilic membrane, which does not adsorb proteins and is easy to clean (Rolchigo et al., 1988).

Results and Discussion

Influence of membrane permeability

The CP model implies that membrane properties do not affect flux beyond a certain pressure. According to Le and Howell (1985), such behavior is not observed in practice. The applicability of the CP model was tested by comparing the flux performance of two membranes with the same nominal molecular weight cut-off, but with different permeabilities. Figure 3 shows that up to 3 bar, the flux increases linearly with pressure and the slope of the line is proportional to the permeability. A further increase in pressure narrows the gap, and at about 10 bar performance is comparable. This result is consistent with the CP model and the conclusion that membrane permeability does not affect performance in the pressure-independent region of maximum flux. An examination of the results suggests a possible explanation for the contradiction noted by Le and Howell (1985). The pressure-independent region was reached at different pressures and in this case at high pressures. Thus, it can be misleading to compare flux rates at the same transmembrane pressure difference. For the membrane with the larger permeability, the pressure-independent region is reached at a pressure around 6 bar. Although the membrane permeability does not affect maximum flux, it determines the pressure at which the maximum flux is reached. Lower permeabilities mean that higher pressures are required to reach the maximum flux.

Approximation of the layer concentration

The filtration of proteins leads to the formation of a CP solute layer on the membrane surface behaving as part of the membrane. The concentration of this layer depends on the size, shape and degree of hydration of the solute (Cheryan, 1986). For the experimental determination of the mass transfer coefficient k in the boundary layer, it is necessary to know the solute concentration c_l, since it determines the driving force for diffusive transport back into the bulk solution.

The procedure commonly used to approximate c_l assumes

the diffusivity D to be constant; therefore, the CP model for flux F is expressed as:

$$F = k \ln \frac{c_l}{c_b} \tag{8}$$

This implies that at $F=0$, $c_l = c_b$. Accordingly, a plot of flux vs. the log of bulk concentration is a straight line and intercepts the abscissa at $c = c_l$. The slope of this line represents k. The value of c_l does not depend on k, since it is a material property. This has experimentally been shown to be true in many cases (Cheryan, 1986); c_l values reported for BSA using this method are between 200 and 300 g/L. This method, however, has several flaws: diffusivity is often a function of concentration; hence, $f(c)$ is not $\ln(c_l/c_b)$. Data gathered for this procedure are obtained by experiments at constant operating conditions for different bulk concentrations. This violates the necessary condition that k be constant, because viscosity rises with increased bulk concentration. In some cases, it is questionable whether all the data used, especially for low bulk concentrations, were obtained in the pressure-independent region.

The procedure used here attempts to correct for the above problems. The concentration dependence of the diffusivity is included in the term $f(c)$. If one assumes that c_l is the same for experiments with similar values of c_b, then c_l can be calculated by the following equation.

$$\frac{F_1}{F_2} = \frac{k_1}{k_2} \frac{\left(\ln \frac{c_l}{c_{b1}} + b(c_l - c_{b1}) \right)}{\left(\ln \frac{c_l}{c_{b2}} + b(c_l - c_{b2}) \right)} \tag{9}$$

At this point, the absolute value of k is not known, but as discussed earlier, k can be expressed by an equation with the following form:

$$k = \left(\frac{D}{d_h} \right) A \, Re_t^a \left(\frac{d_h}{R} \right)^b Sc^c Re_a^d \tag{10}$$

With the exception of the Schmidt number, the dimensionless numbers were kept constant by adjusting the operating parameters. Increasing the concentration in the bulk solution increases the viscosity, causing a decrease in both Re_t and Re_a; this can be compensated by increasing the tangential speed of the rotating membrane and the axial speed of the fluid. The Schmidt number does not depend on operating conditions. Using a heat-mass transfer analogy, the exponent c can be assumed to be 0.33, which is experimentally confirmed for a large range of Schmidt numbers by Mizushina (1971). Incorporating this value into Eq. 9 yields:

$$\frac{F_1}{F_2} = \frac{v_1^{\frac{1}{3}} \left(\ln \frac{c_l}{c_{b1}} + b(c_l - c_{b1}) \right)}{v_2^{\frac{1}{3}} \left(\ln \frac{c_l}{c_{b2}} + b(c_l - c_{b2}) \right)} \tag{11}$$

Equation 11 was used to calculate c_l by iteration. No correction for the concentration dependence of the diffusivity is required, since the term $f(c)$ incorporates the dependence of the diffusivity on the concentration. Table 1 lists the values for the flux (from Figure 4) used for the calculation of c_l. The experiment with a bulk concentration of 10 g/L was not included, since the pressure-independent region was not reached (see Figure 4). Table 2 lists the calculated values for c_l. The first column gives the pair of bulk concentrations used and the second column lists the iterated values for c_l. Columns 3 and 4 show the sensitivity of the iterated values of c_l to changes in the flux values. In column 3, F for the lower c_b was increased by 0.5% and F for the higher c_b was decreased by 0.5%, whereas in column 4, F for the lower c_b was decreased and F for the higher c_b was increased. Obviously, c_l is very sensitive to a change in flux values, especially for lower and higher c_b's.

Table 1. Measured Flux for Different Bulk Concentrations*

c_b g/L	20	30	40	60	90	120	150	200
F, L/h/m^2	119.0	100.4	88.2	70.9	54.7	42.4	35.3	33.0

*$Re_t = 7{,}000$; $Re_a = 50$; $d/R = 0.096$; pH 7.4; $\Delta p = 12.2$ bar.

Table 2. Calculated Values for c_l Using Eq. 11*

c_{b1}/c_{b2} (g/L)/(g/L)	c_l g/L	c_l {1.005*F_1 0.995*F_2}	c_l {0.995*F_1 1.005*F_2}
20/30	203	185	226
30/40	233	209	264
40/60	234	221	248
60/90	255	246	265
90/120	248	242	255
120/150	304	296	313
150/200	549	526	574

*Columns 3 and 4 indicate sensitivity of c_l to changes in flux values.

The values in Table 2 may suggest that c_l rises with increasing bulk concentration contrary to the assumption of the CP model

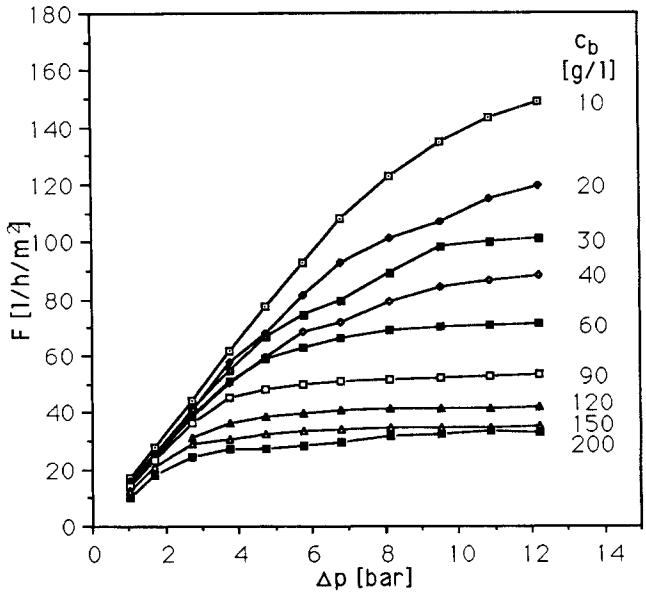

Figure 4. Flux vs. Δp for different bulk concentrations.

$Re_t = 7{,}000$; $Re_a = 50$; $d/R = 0.096$; pH = 7.4. To keep Re_t constant the rotation rate was increased from 700 rpm for 10 g/L to 1,760 rpm for 200 g/L, and to keep Re_a constant the feed rate was increased from 0.22 L/min to 0.56 L/min.

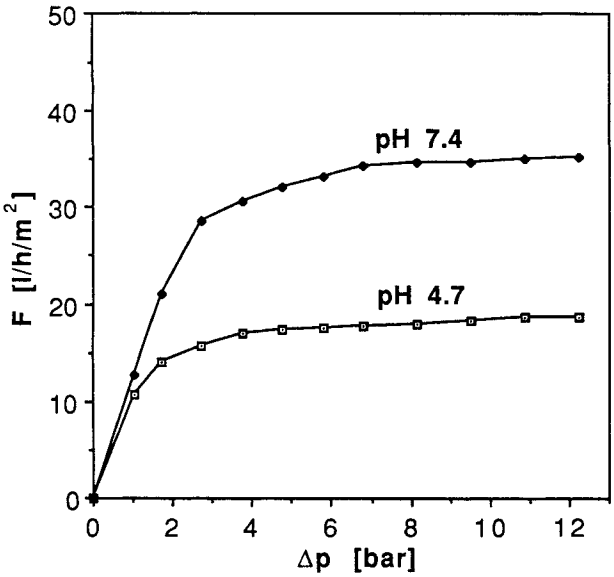

Figure 5. Flux vs. pressure for pH 4.7 and 7.4.

$c_b = 150$ g/L; $Re_t = 7{,}000$; $Re_a = 50$; $d/R = 0.096$.

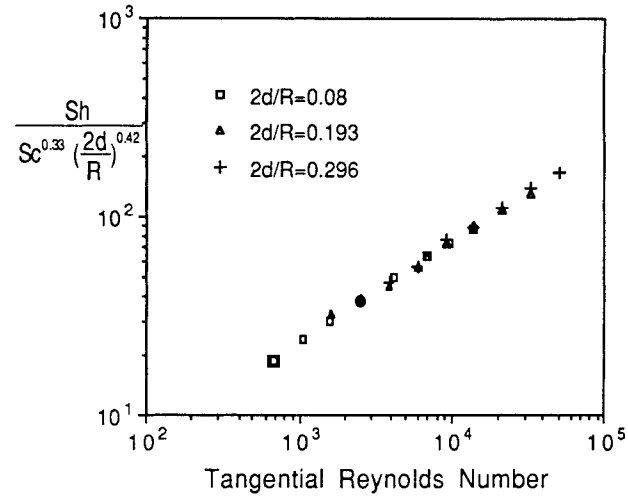

Figure 6. Modified Sherwood number vs. Re_t.

Determined with $c_b = 90$ g/L; $\Delta p = 10.2$ bar.

that c_l is a constant for a given protein. However, c_l is very sensitive to variation in F (Table 2). Furthermore, the equation for the concentration dependence of the diffusivity is experimentally confirmed only for concentrations up to 200 g/L. Since the calculated values for c_l are larger than 200 g/L, the extrapolation to larger concentrations may introduce errors. For $c_{b1}/c_{b2} = 150/200$, the calculated value for c_l is certainly too high since it exceeds the solubility limit of BSA.

Influence of pH

Flux can be described by an equation of the form: $F = k^* f(c)$. The mass transfer coefficient k is calculated using the diffusivity at infinite dilution, since the concentration dependence is included in $f(c)$. Experiments were performed in which $f(c)$ was selectively varied:

- At pH 7.4 and 0.15 M NaCl: $f(c) = \ln(c_l/c_b) + 0.0019(c_l - c_b)$
- At pH 4.7 and 0.1 M acetate buffer: $f(c) = \ln(c_l/c_b) - 0.0021(c_l - c_b)$

The results shown in Figure 5 indicate that flux does not depend on pH for low pressures. For high pressures the difference is considerable. Table 3 compares values obtained for pH 7.4 and 4.7 for different bulk concentration. By forming the ratio of the right sides of Eq. 4, the experimental result can be compared with the theoretical prediction. Since the viscosity does not depend on pH, k cancels. As shown in Table 2, the concentration in the CP layer for pH 7.4 is approximated to 250 g/L for a BSA concentration of 90 g/L. Since c_l may depend on pH, c_l was approximated for pH 4.7 using the values given in Table 3 and the procedure described in the preceding paragraph. For bulk concentrations of 90 and 120 g/L, c_l was calculated to be 338 g/L and for bulk concentrations of 120 and 150 g/L, c_l was calculated to be 355 g/L. Using an average value of 347 g/L for pH 4.7 and 250 g/L for pH 7.4, the theoretical ratios were calculated as shown in Table 3. The experimental ratios are in good agreement with the theoretical ratios given in column 4 of Table 3. It should be mentioned that the equations for the concentration dependence is experimentally confirmed only for concentrations up to 200 g/L.

Table 3. Comparison of F at different pH*

c_b g/L	$F_{\text{pH 7.4}}$ L/h/m²	$F_{\text{pH 4.7}}$ L/h/m²	$\frac{F_{\text{pH 7.4}}}{F_{\text{pH 4.7}}}$	$\frac{f(c)_{\text{pH 7.4}}}{f(c)_{\text{pH 4.7}}}$
90	54.7	31.4	1.74	1.64
120	42.4	24.0	1.77	1.68
150	35.3	18.7	1.89	2.10

*$Re_t = 7{,}000$; $Re_a = 50$; $d/R = 0.096$; $\Delta p = 12.2$ bar. Column 4 shows theoretical ratios.

The values for c_l at pH 4.7 are considerably higher than the values for c_l at pH 7.4, which is to be expected considering the dependence of net charge on pH. At pH 4.7 BSA has no net charge, whereas at pH 7.4 BSA has a net charge of -20. Consequently, the molecules tend to repel each other at pH 7.4 resulting in a lower c_l. No net charge at pH 4.7 allows for closer packing and higher c_l.

Determination of the mass transfer coefficient

The values of the exponents a, b, and d for Eq. 7 were determined by varying the operating conditions and gap width. No influence of axial velocity on flux was observed in the range of gap widths and rotational speed investigated. A likely explanation for this observation is that the rotational velocity is one to two orders of magnitude larger than the axial velocity. The hydrodynamics are determined primarily by rotational, rather than axial, velocity. As a consequence, Re_a is not important under the conditions investigated and $d = 0$.

The exponent a was determined by varying the rotational velocity. The exponent b was obtained through variation of the ratio $2d/R$. The following equation is a fit of the data collected from experiments with a bulk concentration of 90 g/L (Figure 6). The protein concentration in the CP layer was taken as 250 g/L (see Table 2).

$$Sh = 0.75\, Re_t^{0.5} \left(\frac{2d}{R}\right)^{0.42} Sc^{0.33} \qquad (12)$$

The standard deviation is 2.2%, and the correlation was

Table 4. Values for Constant A and Exponent a in Eq. 13

Authors	A	a	Operating Range			
			d/R	Re_a	Ta	Sc
Coeuret (1981)	0.38	0.5	0.143,0.286	30–800	135–3,700	1,380–6,450
Inner Cylinder	0.59	0.5	0.429	"	"	"
Kataoka (1977) Outer Cylinder	0.43	0.49	0.62	0	100–9,200	3×10^3–8×10^5
Mizushina (1971) Outer Cylinder	0.74	0.5	0.62,0.82	0	59–19,500	3×10^3–7.7×10^5
López-Leiva (1979) Inner Cylinder	0.07	0.64	0.143	150	450–3,500	$\approx$17,000
This Work, Eq. 16 Inner Cylinder	0.93	0.5	0.04–0.148	25–300	68–9,740	21,600

determined for: $25 < Re_a < 200$; $0.04 < d/R < 0.148$; and $Sc = 21{,}600$. For $d/R = 0.04$, 0.096, 0.148 Re_t was between 680 and 13,600, 1,650 and 33,000, and 2,530 and 50,600, respectively. This corresponds to Taylor numbers (Eq. 14) between 68 and 1,360, 256 and 5,120, and 487 and 9,740, respectively.

The presented equation should be applicable to all bulk concentrations and solutes. To calculate F with Eqs. 12 and 4, however, information about c_l is necessary. Ideally, the concentration dependence of the diffusivity is also required to determine the form of the term $f(c)$ in Eq. 4. One may estimate c_l with reasonable accuracy for any given solute. In terms of concentration dependence, however, no data will be available in many cases and one will have to assume D to be constant and use Eq. 5 for the term $f(c)$.

Comparison with published data for rotating systems

A commonly-used experimental technique for determination of mass transfer coefficients is an electrochemical method that uses the rate of current discharged on cylindrical electrodes (Mizushina, 1972). In comparison, we measured the permeate flux through a semipermeable membrane, which includes a radial component of the fluid velocity not present in the case of a nonporous wall. Another feature distinguishing our approach from the electrochemical method is the formation of a CP layer on the membrane surface. Since the radial velocity is several orders of magnitude lower than the tangential velocity at the membrane surface, one would expect little or no influence of radial velocity on the mass transfer coefficient.

Published mass transfer correlations express the Sherwood number as a function of the Taylor number and the Schmidt number:

$$Sh = A\ Ta^a Sc^{0.33} \tag{13}$$

$$Ta = \frac{\omega R d}{v}\left(\frac{d}{R}\right)^{0.5} \tag{14}$$

Table 4 is a compilation of the values of the constant A and the exponent a for Eq. 13. The values were determined with electrochemical methods except for López-Leiva, who used filtration of BSA. The Sherwood correlation developed here and written as Eq. 12 uses a set of four dimensionless numbers $\{Sh, Re_t, Sc, 2d/R\}$, while Eq. 13 contains only three dimensionless numbers $\{Sh, Ta, Sc\}$.

To compare the results, Eq. 12 is rearranged and expressed in terms of the Taylor number:

$$Sh = 1.26\ Ta^{0.5}\left(\frac{2d}{R}\right)^{0.17} Sc^{0.33} \tag{15}$$

If the factor $2d/R$ had not been used, the data would have yielded:

$$Sh = 0.93\ Ta^{0.5} Sc^{0.33} \tag{16}$$

The standard deviation increases from 2.2% in Eq. 15 to 16.2% in Eq. 16. A deviation of 16.2% is still an acceptable number considering the usual large scattering found in heat/mass transfer correlations. However, the representation with four dimensionless numbers is considerably more accurate. In the following, it is shown that this representation is consistent with dimensional analysis.

Dimensional analysis was utilized to derive Eq. 7, which is the precursor of Eqs. 12 or 15. Six parameters appear in Eqs. 12 and 13: k, v, D, ω, R and d_h. There are two independent equations for the dimensions of length and time, thus a com-

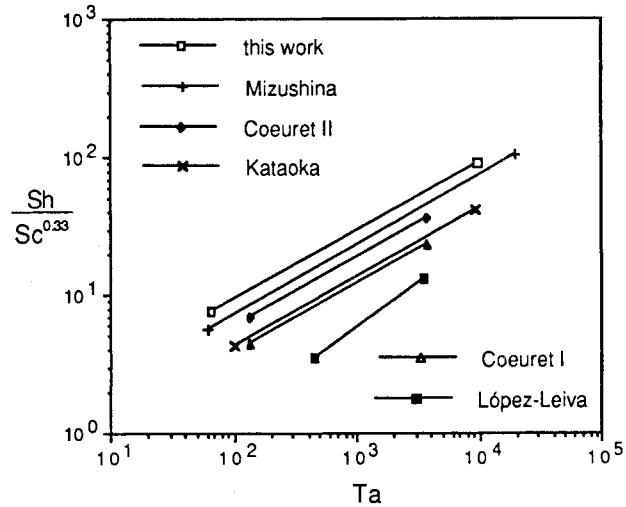

Figure 7. Comparison of different Sherwood correlations in the range of Taylor numbers.

See Table 4.

Table 5. Characteristic Dimensions and Operating Conditions for Various Filtration Systems*

	Δp	$p_{in}-p_{out}$	Dimensions	v, m/s	Re $v=2\times10^{-6}$m^2/s
Tubular Modules	3–25 bar	2 bar for $d=1.25$ cm, $L=2.4$m $v=2$ m/s Skim Milk	$d_h\approx1.5$ cm, L up to 3 m	2–6	15,000–45,000 Turbulent
Hollow Fiber	<2.3 bar	0.9 bar for $d=0.11$ cm, $L=0.64$ m $v=1$ m/s Skim Milk	$d_h=0.2$–1.1 mm, $L=0.2$–1 m	0.5–2.5	50–1,630 Laminar
Plate Frame	15 bar	Stack of 30 Plates 10 bar, $v=2$ m/s	$d=0.4$–1 mm, $L=0.06$–0.6 m	≈2	800–2,000 Laminar
Spiral Wound	>10 bar	1–1.3 bar for $d\approx0.9$ mm, $L=1.1$ m $v=0.25$ m/s	$d=0.7$–1.1 mm, $L=0.3$–2 m	0.1–0.6	70–660 Spacer Mesh Creates Turb.

*Collected by Cheryan (1986), pp. 160, 167, 224).

plete description of the problem requires up to four dimensionless numbers. Accordingly, the set {*Sh*, *Sc*, *Ta*} may be incomplete. If data obtained by experiments without varying d/R is fitted to the partial set {*Sh*, *Sc*, *Ta*}, then no contradiction should be found. This is the case for two of the four equations shown in Table 2.

Figure 7 compares the different correlations in their respective range of Taylor numbers. For this purpose, Eq. 16 is used to represent the results of this work, since Eq. 15 cannot be represented in a way that allows direct comparison. From Figure 7, the Sherwood number correlation developed here yields numbers on the upper end. However, the differences are small enough to allow the conclusion that the mass transfer coefficient determined in our filtration system is in good accordance with correlations developed using a completely different method.

The López-Leiva equation yields considerably lower values. It is based on experiments with BSA concentrations in the range from 0.5 to 5 g/L. The pressures at which these experiments were performed are not mentioned; however, the maximum pressure reported throughout his thesis was 5 bar. The membrane permeabilities were not larger than the permeabilities of the membranes used here. Therefore, the pressures necessary to reach the pressure-independent region are about the same as those required for our experiments. For a tangential Reynolds number of 7,000 (corresponding to a Taylor number of 1,080 for the used d/R), Figure 4 shows that a pressure of 12 bar was not sufficient to reach maximum flux for a bulk concentration of 10 g/L, and even a bulk concentration of 60 g/L requires pressures around 8 bar. Accordingly, the lower values of the López-Leiva equation may be due to the fact that experiments were not performed in the pressure-independent region.

Comparison of different filtration configurations

Different filtration systems can be compared by calculating k using the appropriate correlations assuming that c_l is solute-specific and independent of the filtration configuration. The characteristic dimensions and operating conditions taken from Cheryan (1986) and used here are summarized in Table 5.

The mass transfer coefficient in turbulent flow was calculated using the correlation of Dittus and Boelter:

$$Sh=0.023\ Re_a^{0.8}\ Sc^{0.33} \tag{17}$$

The quantitative estimation of flux from this equation for macromolecular solutions was found to be in good agreement with experimental data for human albumin (Porter, 1972). This is also the case for the Graetz-Lévêque correlation for laminar flow in thin channels:

$$Sh=1.62\left(Re_a\,Sc\,\frac{d_h}{L}\right)^{0.33} \tag{18}$$

The range of mass transfer coefficients calculated with Eqs. 17 and 18, as well as the numbers compiled in Table 4, are represented in Table 6. The mass transfer coefficient in vortex flow filtration was calculated with Eq. 12.

Because of pressure limitations in hollow-fiber systems, filtration will not take place in the pressure-independent region. Thus, the values given in Table 6 are an upper limit. The range of Reynolds numbers for spiral-wound modules indicate that the flow is laminar; however, spacers will introduce some turbulence-enhancing mass transfer. Therefore, Table 6 gives values for both laminar and turbulent case, which can be considered lower and upper limit, respectively.

According to this calculation, vortex flow filtration outperforms all other configurations except for tubular units that are comparable. To achieve high performance in tangential flow filtration, a considerable pressure drop is created to move the liquid at a high velocity. The typical pressure drop of a tubular module was calculated to be 2 bar for operation at a velocity of 2 m/s (Table 5). Pressure drop is proportional to

Table 6. Estimated Range of Mass Transfer Coefficients for Filtration Systems in Table 5*

Configuration	Equation	$k\times10^6$ m/s
Tubular Module	17	6.5–16
Hollow Fiber	18	<(1.7–9.9)
Plate and Frame	18	2.9–4.0
Spiral Wound	18	0.9–2.8
	17	1.0–4.0
Vortex Flow	12	5.4–26

*$D=6*10^{-11}$ m^2/s; $\nu=2*10^{-6}$ m^2/s

the square of the velocity. For a velocity of 6 m/s, at which the maximum k for the tubular unit was calculated, we expect a pressure drop of 18 bar. The large value of k has to be paid for with a very high pressure drop and, consequently, a reduced average transmembrane pressure difference.

The performance of rotary filtration is disconnected from the axial Reynolds number in the range investigated. Consequently, flux does not depend on the feed rate. The unit can be operated at very low feed rates with a negligible pressure drop, and hence low energy consumption for pumping. Furthermore, low feed flow rates minimize the damage to the product due to pump action, which can be of considerable importance with shear-sensitive products.

Conclusions

The experimental data suggest that the CP model is a valid approach to ultrafiltration in a vortex flow configuration. The most prominent experimental evidence is that flux ceases to depend on membrane permeability beyond a threshold pressure. Beyond this threshold pressure, flux can be described without membrane properties as predicted by the CP model.

In the theoretical approach, the CP model was modified to include the concentration dependence of the diffusivity. This approach yields the relation $\mathbf{F = k^*f(c)}$, where k is a characteristic of the filtration configuration and $f(c)$ is solute-specific. This approach is consistent with experiments, in which k was kept constant and the term $f(c)$ was varied selectively by changing the pH of the solution. The theoretical prediction is in good agreement with the strong dependence of flux on pH as found experimentally.

A prerequisite for the application of the CP model is the knowledge of the protein concentration adjacent to the membrane surface (c_l). This concentration is assumed to be constant for each protein, and therefore independent of bulk concentration and hydrodynamics. The method usually applied to approximate c_l has several flaws. Consequently, in the present study, the method was altered. The results show that c_l depends on the pH of the solution that can be attributed to changes in the net charge. The results also suggest that c_l may depend on c_b. Using the approximated c_l, a Sherwood number correlation was determined to describe the data. Since the CP model suggests that filtration can be described by mass transfer, the correlation is compared with published correlations derived using electrochemical methods used to measure mass transfer from a rotating cylinder. The absolute values were found to be in general agreement, thereby supporting the validity of the CP model. It, however, was found that our results could be represented much better by an equation with an additional dimensionless number, the inclusion of which could be justified through the dimensional analysis.

Using the developed correlation, it was shown that filtration performance in rotary devices is superior to that obtainable in cross-flow filtration (CFF) devices. Another feature distinguishing VFF from CFF is that performance was independent of the feed rate in the investigated range; this allows VFF to be operated effectively at very low feed rates, with a negligible pressure drop, whereas conventional crossflow devices require high feed velocities with consequent high pressure drops to achieve high flux values.

Acknowledgment

Ulrich Holeschovsky thanks the Ernest-Solvay Foundation for a fellowship support, the Biotechnology Process Engineering Center which is supported by the National Science Foundation under the Engineering Research Center Initiative (Cooperative Agreement CDR-88-03014), and Membrex Inc. for financial support and equipment. Appreciation also goes to Phil Rolchigo, Arun Chandavarkar, Robert S. Murray, Gopal Agarwal, Jim Hildebrandt, Kay Herbert, and Jerome Sullivan for their help and advice.

Notation

b = constant
c = concentration, g/L
c_b = bulk concentration, g/L
c_l = layer concentration, g/L
d = gap width, m
d_h = hydraulic diameter, m
D = diffusivity, m^2/s
D^o = diffusivity at infinite solution, m^2/s
F = volumetric flux, $L/h/m^2$
k = mass transfer coefficient, m/s
L = length, m
p = permeability, $L/h/m^2/bar$
R = radius of the inner cylinder, m
v = axial fluid velocity, m/s
x = coordinate perpendicular to membrane surface, m

Greek letters

ρ = density, kg/m^3
μ = dynamic viscosity, kg/m/s
μ_w = dynamic viscosity of pure water, kg/m/s
ν = kinematic viscosity, m^2/s

Literature Cited

Cheryan, M., *Ultrafiltration Handbook*, Technomic Publishing Co. (1986).

Coeuret, F., and J. Legrand, "Mass Transfer at the Electrodes of Concentric Cylindrical Reactors Combining Axial Flow and Rotation of the Inner Cylinder," *Electrochimica Acta*, **26**(7), 865 (1981).

Fair, B. D., D. Y. Chao, and A. M. Jamieson, "Mutual Translational Diffusion Coefficients in Bovine Serum Albumen Solutions Measured by Quasielastic Laser Light Scattering," *J. of Colloid and Interf. Sci.*, **66**(2), 323 (1978).

Kataoka, K., H. Doi, and T. Komai, "Heat/Mass Transfer in Taylor Vortex Flow with Constant Axial Flow Rates," *Int. J. of Heat Mass Transf.*, **20**, 57 (1977).

Kozinski, A. A., and E. N. Lightfoot, "Protein Ultrafiltration: A General Example of Boundary Layer Filtration," *AIChE J.*, **18**(5), 1030 (1972).

Le, S. M., and J. Howell, *Ultrafiltration, Comprehensive Biotechnology*, Vol. 2, Pergamon Press (1985).

López-Leiva, M., "Ultrafiltration in Rotary Annular Flow," Doctoral Diss., Univ. of Lund, Sweden (1979).

Mizushina, T., "The Electrochemical Method in Transport Phenomena," *Adv. in Heat Transf.*, **7**, 87 (1971).

Nakao, S. I., T. Nomura, and S. Kimura, "Characteristics of Macromolecular Gel Layer Formed on Ultrafiltration Tubular Membrane," *AIChE J.*, **25**(4), 615 (1979).

Porter, M. C., "Concentration Polarization with Membrane Ultrafiltration," *Ind. Eng. Chem. Prod. Res. Develop.*, **11**(3), 234 (1972).

Rolchigo, P., W. Raymond, J. Hildebrandt, "The Improved Control of UF with the Use of Vorticular Hydrodynamics and Ultra-Hydrophilic Membranes," AIChE Meeting, Washington, DC (Dec., 1988).

Vilker, V. L., C. K. Colton, and K. A. Smith, "Theoretical and Experimental Study of Albumin Ultrafiltered in an Unstirred Cell: II." *AIChE J.*, **27**(4), 642 (1981).

Manuscript received Dec. 12, 1990, and revision received July 8, 1991.